Appl. Phys. B (2015) 118:295–307
DOI 10.1007/s00340-014-5986-8

Applied Physics B
Lasers and Optics

Temporally and spectrally resolved UV absorption and laser-induced fluorescence measurements during the pyrolysis of toluene behind reflected shock waves

S. Zabeti · A. Drakon · S. Faust · T. Dreier · O. Welz · M. Fikri · C. Schulz

Received: 13 October 2014 / Accepted: 15 December 2014 / Published online: 31 December 2014

Abstract Toluene is frequently used as fluorescence tracer in high-temperature combustion applications. A quantitative analysis of laser-induced fluorescence (LIF) signals requires the knowledge of photophysical properties and decomposition kinetics. Using spectrally and temporally resolved ultraviolet absorption and LIF measurements, we studied the spectral properties of toluene and its pyrolysis products behind shock waves between 810 and 1,755 K. Transient absorption spectra were acquired between 220 and 300 nm. The temporal behavior of the absorption at 266 nm was compared to simulations based on literature kinetics models of toluene pyrolysis and available high-temperature absorption cross-sections of toluene, benzyl radicals, and C_7H_6 as a product from benzyl decomposition. Experiment and simulation agree well at the beginning of the pyrolysis process, whereas for longer reaction times deviations occur presumably due to the build-up of high molecular weight species, which contribute to the observed absorption but have unknown spectral properties. Additionally, LIF emission spectra were recorded following 266-nm excitation at selected reaction times. From measurements up to 1,220 K, the relative fluorescence quantum yield of toluene was derived, extending existing data to higher temperatures. Products from toluene pyrolysis were found to be the major contributors to the LIF signal at higher temperatures.

S. Zabeti · S. Faust · T. Dreier · O. Welz · M. Fikri · C. Schulz (✉)
IVG, Institute for Combustion and Gas Dynamics – Reactive Fluids, University of Duisburg-Essen, Duisburg, Germany
e-mail: christof.schulz@uni-due.de

A. Drakon
Institute for High Energy Density, Russian Academy of Sciences, Moscow, Russia

1 Introduction

Tracer-LIF (laser-induced fluorescence) diagnostics based on organic fluorescent tracers such as toluene, acetone, or 3-pentanone is frequently used for imaging measurements of fuel concentration, equivalence ratio, and temperature in combustion processes [1–5]. Here, a small amount of the tracer is mixed with a non-fluorescing fuel, and its fluorescence intensity after laser excitation is recorded to monitor the distribution of the evaporated fuel from the signal intensity or to derive information about local temperature and oxygen partial pressure based on relative signal intensities in multicolor measurements. To provide the data required for the quantitative interpretation of the measured signal, absorption cross-sections, fluorescence quantum yields, and fluorescence spectra of various tracer species have been investigated for a wide range of pressure and temperature in heated flow cells [2, 6, 7]. In modern highly energy-efficient internal combustion (IC) engines with high compression ratios or in homogeneous charge compression ignition (HCCI) engines, however, high in-cylinder temperatures raise concerns about the thermal stability of the tracer throughout the measurement cycle [8]. Under such conditions, the tracer can pyrolyze or oxidize over the observation timescale, which can significantly influence the interpretation of the tracer fluorescence signals.

For practical tracer applications in IC engines, it must be known whether the tracer represents the parent fuel reliably (i.e., decomposes and is oxidized at the same rate as the fuel). In this case, close to autoignition, the tracer would disappear early in the cool-flame phase before the onset of heat release. Alternatively, a tracer could represent the total amount of non-oxidized fuel even after the parent fuel molecules have been consumed. In this second case, the tracer would stay present and would only disappear after the

onset of hot ignition [8]. Simulations have indicated that the decomposition and ignition behavior of fluorescence tracers can differ significantly from the behavior of the parent fuel [9, 10]; these effects strongly depend on the chemical structure of the tracer. Additionally, potential decomposition products may contribute either to absorption (leading to laser and signal attenuation) or even fluorescence (forming a potential source of interference or opening new diagnostics opportunities). Therefore, detailed investigations of the optical properties of tracers and their decomposition products during their thermal degradation are necessary for the quantitative interpretation of tracer-LIF measurements under IC engine conditions at high temperatures. An additional concern is the potential interaction of tracers with the ignition chemistry of the parent fuel, which may affect the ignition and combustion properties of the parent fuel [11, 12].

Experiments in HCCI engines have shown that the tracer 3-pentanone disappears several hundred microseconds before autoignition and additional species (here: formaldehyde) are formed during the ignition of the fuel/air mixture [8]. Longer-chain ketones, such as 5-nonanone, have shown significant changes in fluorescence spectra indicating tracer decomposition in a diesel environment where, however, non-specified fluorescing decomposition products compensated for the loss of the original tracer [13].

Experimental studies of tracer decomposition that would provide the required kinetics and spectroscopic data are sparse and have often been carried out in application-motivated environments without perfect control of the reaction conditions [8, 13, 14]. Detailed spectroscopic data required for the interpretation of tracer fluorescence intensities in an engine environment are typically gained from experiments in heated high-pressure cells. These cells can be operated either in stationary [6] or in continuous flow mode, in which the mixture of tracer diluted in buffer gas is continuously replaced with fresh gas [15–18]. Under these conditions, stability limits have been evaluated and toluene was found to be more stable than acetone and 3-pentanone [18]. However, even when using flow cells, residence times are on the order of seconds and the limitations concerning the thermal stability of the gas mixture investigated are much more stringent than for applications in engine environments, where stability on the order of milliseconds is sufficient. Therefore, studies in heated cells are limited to temperatures below the maximum temperatures (~1,300 K) of interest for IC engines.

Because of the rapid gas-dynamic heating of gases within a few microseconds, shock tubes give access to spectral measurements on shorter timescales (observation times in our setup of up to ~1.5 ms) and at higher temperatures compared to heated cells. Whereas shock tube setups have already been used to measure absorption cross-sections of toluene up to 1,130 K [19] and between 1,400 and 1,780 K [20], they also enable the observation of absorption and fluorescence from products formed from the tracer decomposition. The obtained spectra and the temporal variation of effective absorption cross-sections provide a valuable data base for practical applications in high-temperature environments and can also serve as validation targets for chemical kinetics modeling of the different reaction steps during tracer decomposition. Thus, shock tube studies contribute to the interpretation of the entire tracer decomposition process with regard to interfering species.

This paper focuses on toluene, which is frequently used as a fluorescent tracer for engine applications because of its strong fluorescence signal and its natural occurrence in commercial gasoline (typically 5–15 vol. %) [21, 22]. The limited thermal stability of toluene at high temperature has restricted previous experiments on its spectral properties in flow cells to temperatures below 1,100 K [19, 23] to avoid decomposition on the experimental timescales. In this paper, we focus on O_2-free pyrolytic conditions in our experiments. Due to the lack of efficient fluorescence quenching by O_2 and therefore significantly stronger signals [15], oxygen-free environments are frequently used for high-precision tracer-LIF measurements (e.g., [5]).

Sick and Westbrook [9] have shown that gas-phase decomposition of toluene proceeds with a different rate than the decomposition of typical model fuel components such as *iso*-octane or *n*-heptane. This result highlights the need for accurate knowledge of the pyrolysis and oxidation kinetics of toluene and the spectroscopic properties of its decomposition products.

The kinetics and mechanism of the thermal decomposition of toluene in the gas phase,

$$C_6H_5CH_3 \rightarrow \text{Products}, \tag{R1}$$

have been intensively investigated both experimentally and computationally (e.g., Ref. [24] and references cited therein). The main unimolecular reaction channels of toluene are C–H bond fission (R1a) forming an H atom and the resonance stabilized benzyl ($C_6H_5CH_2$) radical, and C–C bond fission (R1b) producing methyl (CH_3) and phenyl (C_6H_5) radicals:

$$C_6H_5CH_3 \rightarrow C_6H_5CH_2 + H \tag{R1a}$$

$$C_6H_5CH_3 \rightarrow C_6H_5 + CH_3. \tag{R1b}$$

The products of R1a and R1b can undergo subsequent reactions, which need to be accounted for in the kinetics modeling of toluene pyrolysis.

In the present work, UV absorption spectra of toluene and its decomposition products were measured as a function of reaction time behind reflected shock waves. These measurements were compared to and interpreted based on

simulations using two kinetics models for toluene pyrolysis—the mechanism of Oehlschlaeger et al. [20] and the very recently published mechanism of Yuan et al. [25, 26]—and high-temperature absorption cross-sections from Ref. [20]. In addition, the fluorescence behavior of toluene and of the reacting mixture using 266-nm laser excitation was investigated during pyrolysis at selected reaction times and various temperatures.

2 Experiment

Measurements were performed in a stainless-steel shock tube at temperatures between 810 and 1,755 K at pressures between 1.2 and 2.9 bar using mixtures of 0.1–2 % toluene diluted in argon. The shock tube has an inner diameter of 79 mm. The driven section (length 7.3 m) was separated from the driver section (length: 3.6 m) by an aluminum diaphragm (thickness 50–90 µm). The velocity of the incident shock wave was determined from the signal of four piezoelectric pressure transducers (603B, Kistler) placed at various distances from the endwall of the tube. Temperature and pressure behind the reflected shock wave were calculated from the measured initial test gas pressure, temperature, composition, and incident shock wave velocity based on ideal one-dimensional shock equations using the CHEMKIN-II package [27].

Gaseous mixtures of toluene (for analysis grade, Merck Chemicals) in argon (>99.999 %, Air Liquide) were prepared manometrically and were allowed to homogenize at least 12 h before use.

2.1 Absorption measurements

The absorption of toluene was recorded temporally and spectrally resolved using the setup shown in Fig. 1. A deuterium lamp (30 W, Heraeus D200 F-HV) was used as a broadband UV light source. After collimation, the light passed through quartz windows (diameter: 8 mm) mounted in the sidewall of the shock tube located 30 mm upstream of the endwall. After passing the exit window, the light was focused on the entrance slit of the spectrograph (Acton SP 2300i, Princeton instruments, 300 g/mm grating, slit width: 300 µm leading to 5-nm spectral resolution). The spectrograph was coupled to a UV-sensitive back-illuminated EMCCD camera (Ixon, Andor, EM gain: 210, pre amplifier: 1×), which was operated in the so-called kinetic mode: After triggering the camera with the signal from pressure transducer #3 that recorded the passage of the incident shock wave, the collected charges on the CCD were shifted to the adjacent pixel rows perpendicular to the wavelength axis once every 3.2 µs. Only the uppermost six pixel rows of the CCD chip were illuminated

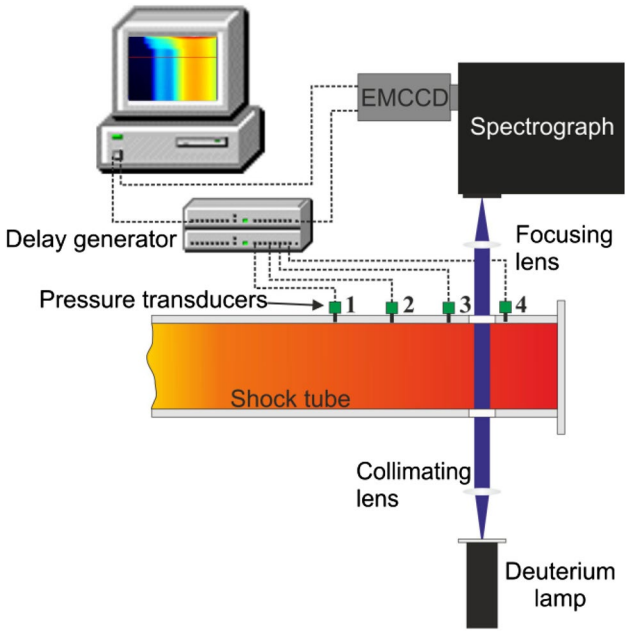

Fig. 1 Experimental arrangement for spectrally and temporally resolved UV absorption measurements of toluene in a shock tube

using a rectangular aperture perpendicular to the entrance slit of the spectrograph resulting in a series of absorption spectra with a fundamental time resolution of 20 µs covering a test time during the shock tube experiment of up to 1.6 ms (note that the observed time resolution was ~70 µs under our operating conditions). Before each experiment, a dark image was taken and subtracted from the measured image. The CCD chip was Peltier-cooled to −12 °C. Data acquisition was synchronized with a delay generator (DG535, Stanford Research Systems) using the signal of the pressure transducer #3 as trigger input (cf. Fig. 1). The wavelength scale of the spectrograph was calibrated using a low-pressure mercury discharge lamp.

Changes in the transmitted light intensity and hence the absorption spectra at various times were investigated by determining the fractional absorption

$$(I_0(\lambda) - I(\lambda, t))/I_0(\lambda). \quad (1)$$

Here, $I_0(\lambda)$ is the wavelength-dependent incident light intensity (signal averaged over 300 times with an empty shock tube) and $I(\lambda, t)$ is the time- and wavelength-dependent transmitted light intensity. The fractional absorption was calculated for specific wavelength ranges from both the incident and transmitted light by binning corresponding pixels on the wavelength axis as a function of time. Figure 2 shows the fractional absorption of the shock-heated mixture as a function of time (y-axis) and wavelength (x-axis) for two different post-shock conditions. Because of the increase in density of the absorbing species behind the reflected shock

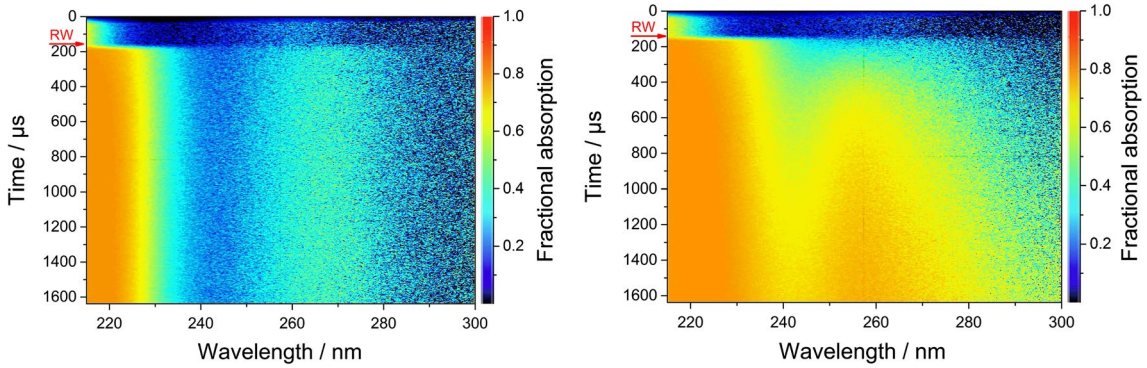

Fig. 2 Temporally and spectrally resolved fractional absorption (raw image) of shock-heated mixture of toluene in Ar. The arrival of the reflected shock wave at the detection volume is marked by "*RW*." Conditions after the reflected shock wave: $T = 1{,}140$ K, $p = 1.5$ bar, 2 % toluene in Ar (*left panel*), $T = 1{,}550$ K, $p = 2.1$ bar, 0.2 % toluene in Ar (*right panel*)

wave, the light transmission decreases immediately, and hence, the fractional absorption increases. The left panel of Fig. 2 shows results from an experiment at 1,140 K, where toluene is stable on the experimental timescale. As a consequence, the absorption spectrum remains constant during the constant high-temperature conditions behind the reflected shock wave. In contrast, the absorption spectrum at 1,550 K changes as a function of reaction time, reflecting decomposition of toluene on the experimental time scale.

At temperatures below 1,200 K where toluene pyrolysis is expected to be insignificant on our experimental timescale, datasets were averaged in the time domain to optimize the signal-to-noise ratio. The absorption cross-section $\sigma(\lambda)$ of toluene was determined according to Beer–Lambert's law,

$$\sigma(\lambda) = -\frac{\ln(I(\lambda)/I_0(\lambda))}{cl}, \tag{2}$$

from the transmitted and incident light intensities $I(\lambda)$ and $I_0(\lambda)$, respectively, the known concentration c of toluene after the reflected shock wave and the path length l (i.e., the inner diameter of the shock tube). The absolute concentration of toluene behind the reflected shock wave was calculated from shock wave equations [28] based on the known mole fraction of toluene in the gas mixture and using the initial pressure (both total pressure and partial pressure of toluene) and temperature in the driven section (T_1 and p_1) and the measured velocity of the incident shock wave. $I(\lambda)$ represents the time-integrated light intensity after passage of the reflected shock wave.

2.2 LIF measurements

The shock tube was alternatively equipped with a system for spectrally resolved measurements of LIF at selected reaction times (cf. Fig. 3). The gas mixture behind the reflected shock wave was excited by a pulsed frequency-quadrupled Nd:YAG laser (Quanta-Ray, Lab-150) at 266 nm with a pulse duration of ~5 ns. The laser beam diameter was reduced by a Galilei telescope to ~7 mm (fluence ~35 mJ/cm^2) and directed through quartz windows in the sidewall of the shock tube 30 mm upstream of the endwall. The laser energy was measured using a power meter (LabMax-TOP, Coherent) during each experiment to assess and correct for laser pulse energy fluctuations. In the single-shot operation of the Nd:YAG laser, fluctuations were typically $\leq$9 %. The emitted fluorescence was collected perpendicular to the laser beam through a quartz window in the endwall of the shock tube and was focused on the entrance slit of a spectrograph (Acton SP 2150i, Princeton Instruments, 150 g/mm grating, 500 µm slit width resulting in a 10-nm spectral resolution) using two fused silica lenses ($f = 160$ and 90 mm). The spectrally resolved light was recorded by an intensified CCD camera (Imager Intense, LaVision, 300 ns gate time).

The wavelength axis of the spectrograph was calibrated using a low-pressure mercury discharge lamp. The emission spectra of a deuterium (for $\lambda < 400$ nm) and a tungsten lamp (for $\lambda > 350$ nm), respectively, with known spectral radiance were used to correct for the wavelength-dependent throughput and camera sensitivity.

Laser and camera were synchronized with the shock wave using a delay generator (DG535, Stanford Research Systems) using the signal of the incident wave recorded by the pressure transducer #4 (cf. Fig. 3) as trigger input. For each shock tube experiment, a single LIF measurement was taken at a selected time after the arrival of the reflected shock wave. The slit of the spectrometer was oriented parallel to the laser beam and thus in principle provided one-dimensional spatial resolution. However, since no spatial variation of the signal is expected for this coordinate, the fluorescence signal of the recorded image was integrated

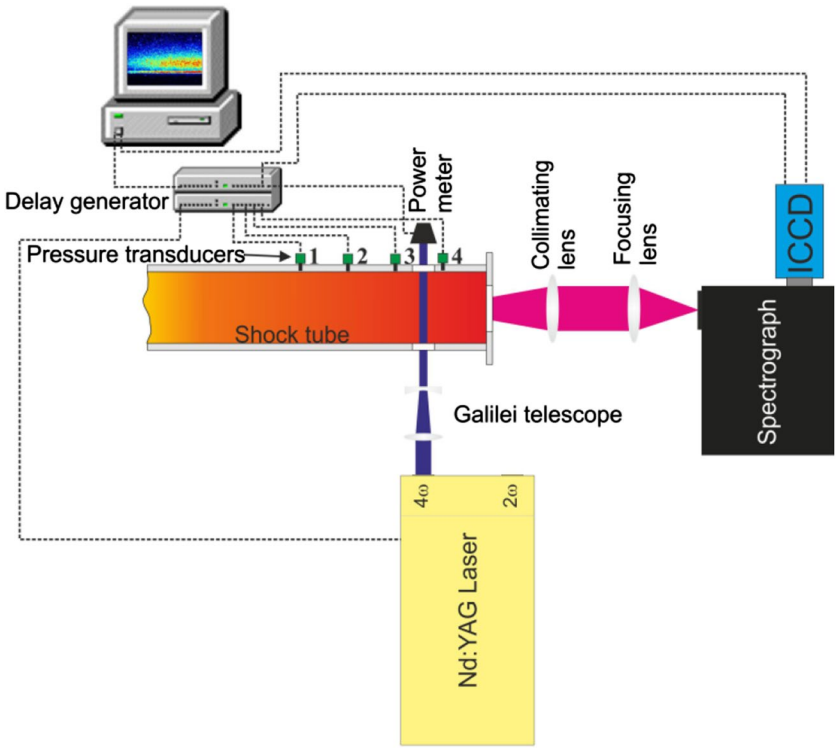

Fig. 3 Experimental setup for the LIF measurements

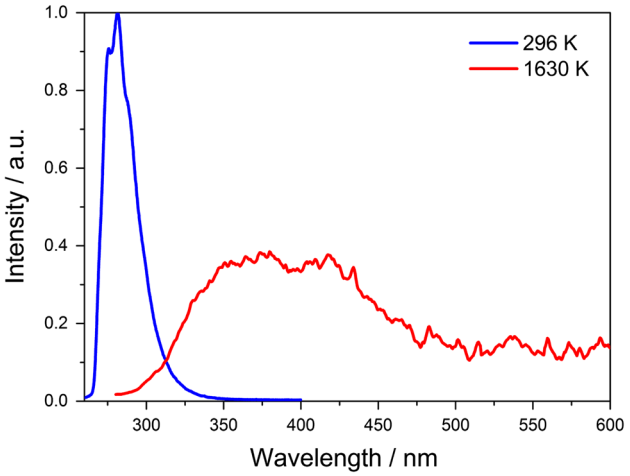

Fig. 4 Single-shot LIF spectra for an experiment with 1 % toluene in Ar. *Blue line*: 296 K, 75 mbar, before the arrival of the shock wave; *red line*: 1,630 K, 2.9 bar, 160 µs after passage of the reflected shock wave

along the slit direction to improve the signal-to-noise ratio. A dark image taken before each experiment was subtracted from the measured image. Figure 4 shows two LIF spectra, one recorded for toluene at room temperature and the other for the reacting mixture at 1,630 K, 160 µs after the reflected shock wave.

The total detected LIF signal intensity of the tracer S_{fl} at a fixed excitation wavelength λ_{ex} and temperature T is proportional to the number density of tracer n_{fl}, the absorption cross-section σ and the fluorescence quantum yield ϕ_{fl}:

$$S_{\mathrm{fl}} \propto n_{\mathrm{fl}} \sigma(\lambda_{\mathrm{ex}}, T) \phi_{\mathrm{fl}}(\lambda_{\mathrm{ex}}, T) \tag{3}$$

If the number density of the tracer is time independent, the combined effects of σ and ϕ_{fl} determine the dependence of the LIF intensity on wavelength and temperature. As a consequence, knowledge of the absolute value and the temperature dependence of the fluorescence quantum yield of tracer species are crucial for quantitative applications.

For weak laser excitation, the fluorescence signal intensity can be calculated from the following equation:

$$S_{\mathrm{fl}} = \frac{I}{hc/\lambda_{\mathrm{ex}}} V n_{\mathrm{fl}} \sigma(\lambda_{\mathrm{ex}}, T) \phi_{\mathrm{fl}}(\lambda_{\mathrm{ex}}, T) \eta_{\mathrm{opt}} \Omega/4\pi \tag{4}$$

where I is the laser fluence, hc/λ_{ex} is the photon energy at the excitation wavelength λ_{ex} in the observed volume V, η_{opt} is the efficiency of the detection system, and $\Omega/4\pi$ is the fractional detection solid angle collected by the lens.

In general, pressure affects the fluorescence quantum yield, albeit in the presented LIF data the pressure was kept constant at 1.2 bar. The detection efficiency η_{opt} and the fractional detection solid angle $\Omega/4\pi$ are constant throughout the measurements with the same setup. According to Eq. (4), the relative fluorescence quantum yield can be derived from the expression

$$\frac{\phi_{\mathrm{fl},T}}{\phi_{\mathrm{fl,ref}}} = \frac{S_{\mathrm{fl},T}}{I_T n_{\mathrm{fl},T} \sigma_T} \frac{I_{\mathrm{ref}} n_{\mathrm{fl,ref}} \sigma_{\mathrm{ref}}}{S_{\mathrm{fl,ref}}}, \tag{5}$$

where the index "ref" represents the quantities determined at reference conditions, typically the lowest temperature investigated (here: 298 K). To obtain the relative fluorescence quantum yield of toluene, the fluorescence signals were integrated between 270 and 370 nm.

3 Results

3.1 Absorption measurements

A series of time-resolved UV absorption spectra of shock-heated toluene diluted in argon was measured between 810 and 1,755 K at pressures of 1.2 and 2.1 bar. Absorption spectra were acquired in the 220–300-nm wavelength range with a spectral resolution of 5 nm. The time resolution was ~70 µs under our operating conditions. Figure 5 shows absorption spectra at various temperatures between 298 and 1,140 K, where decomposition of toluene is negligible on the experimental timescale [29]. At room temperature, the spectrum peaks at ~258 nm with a full width at half maximum (FWHM) of ~25 nm and a peak absorption cross-section of $\sigma_{258\ \mathrm{nm}}$ (298 K) = 4.3 × 10^{-19} cm^2. This spectral feature is caused by the $S_0 \rightarrow S_1$ transition. The room temperature absorption measurements (taken at 150 mbar) are consistent with results from the literature [19, 30]. The strong $S_0 \rightarrow S_2$ transition centered at ~200 nm at room temperature on the blue side of the spectrum (this maximum cannot be captured with the current experimental setup) shows a significant redshift with temperature and overlaps with the $S_0 - S_1$ transition at high temperatures [19]. The entire spectra show a redshift and an increase in the total absorption between 230 and 300 nm with increasing temperature.

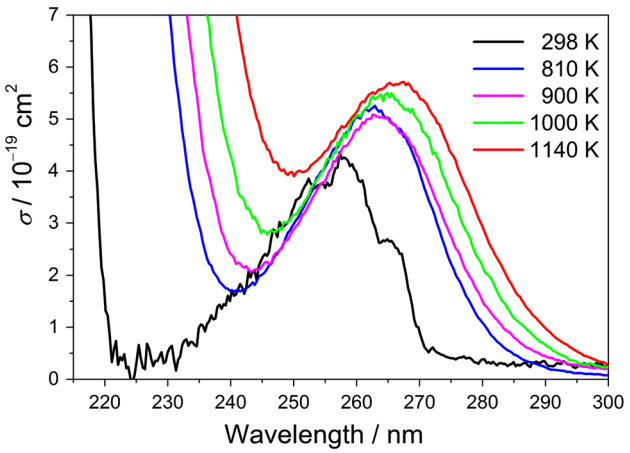

Fig. 5 Absorption spectra of a 2 % mixture of toluene in Ar at room temperature (150 mbar) and at higher temperatures (1.2 bar) according to Eq. 2

Because fluorescence is often excited with standard UV laser sources such as excimer or Nd:YAG lasers, we plot absorption cross-sections at 248 and 266 nm, respectively, as a function of temperature in Fig. 6. At 248 nm, the absorption cross-section is approximately independent of temperature up to 1,000 K and is mostly due to the $S_0 \rightarrow S_1$ transition. Above this temperature, the absorption cross-section increases with temperature. This increase can be rationalized by an additional contribution of the $S_0 \rightarrow S_2$ absorption feature [19], which is accessible due to the increased thermal population of higher vibrational levels in the ground state from where absorption starts. In contrast, the absorption cross-section at 266 nm (right plot in Fig. 6) increases monotonically with temperature up to ~1,100 K. The absorption cross-section at 266 nm at 1,140 K, the upper limit of our determination range, is $\sigma_{266\ \mathrm{nm}}$ = (5.7 ± 0.9) × 10^{-19} cm^2. This value is consistent with results from Oehlschlaeger et al. [20] at higher temperature, who found a temperature-independent value $\sigma_{266\ \mathrm{nm}}$ = (5.9 ± 0.6) × 10^{-19} cm^2 between 1,400 and 1,780 K. Considering the spectral resolution of ~5 nm in our experiment, the obtained cross-sections are globally somewhat lower but in reasonable agreement with existing literature values in the same temperature range [19].

Figure 7 shows the effective absorption cross-sections σ_{eff} at 266 nm at various reaction times after the arrival of the reflected shock wave. σ_{eff} is defined as the cross-section of

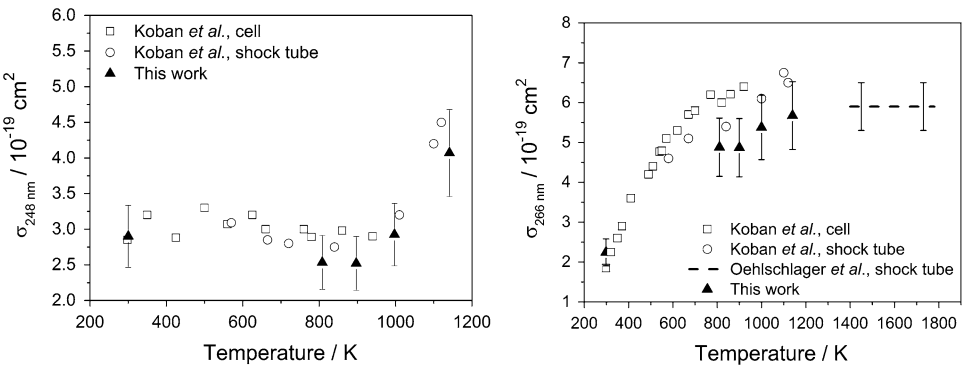

Fig. 6 Absorption cross-sections of toluene at 248 nm (*left panel*) and 266 nm (*right panel*) as a function of temperature. The uncertainty of our determination of 15 % is shown as *error bars*. Results from this study are compared to literature values of Koban et al. [19] and Oehlschlaeger et al. [20]

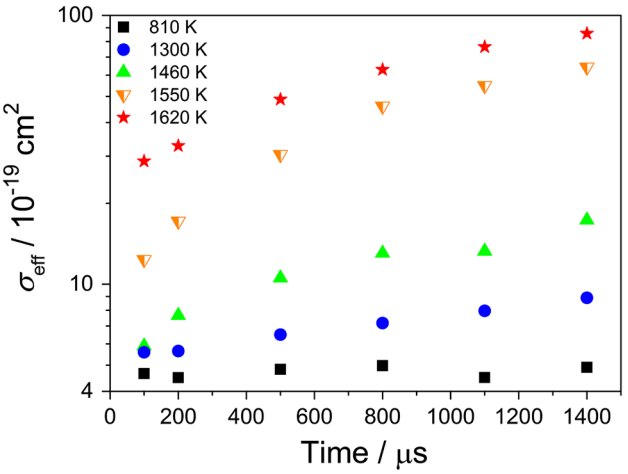

Fig. 7 Measured effective absorption cross-sections σ_{eff} as a function of time after arrival of the reflected shock wave at 266 nm

the mixture based on the initial concentration of toluene after arrival of the reflected shock wave. Below ~1,200 K, σ_{eff} is constant with reaction time and can be assigned to toluene [31]. At 1,300 K and above, σ_{eff} increases as a function of reaction time. Because the absorption cross-section of toluene at 266 nm is independent of temperature between ~1,400 and 1,700 K [20], this result indicates that pyrolysis of toluene becomes important on the experimental timescale and that the products formed are stronger absorbers than toluene. These measurements represent a benchmark for how much absorption increases with temperature, an effect that can be important for laser-based measurements in practical applications where laser beam attenuation must be kept below a specific level.

To gain more insight into which products might contribute to the increased absorption as the temperature increases, we performed chemical kinetics modeling of experiments at 1,550 K (0.1 % toluene, 2.0 bar), 1,620 K (0.1 % toluene, 2.1 bar), and 1,755 K (0.2 % toluene, 2.1 bar) under adiabatic conditions. First, we used the mechanism of Oehlschlaeger et al. [20]. Under their experimental conditions (employing a factor of 5–10 lower toluene concentrations than in our study), Oehlschlaeger et al. could successfully model their observed fractional absorption at 266 nm at early reaction time considering time-dependent contributions of toluene, benzyl radicals, and decomposition products of the benzyl radicals (denoted as C_7H_6):

$$\frac{I_0(\lambda) - I(\lambda,\mathrm{t})}{I_0(\lambda)} = 1-(\exp\,(-l(\sigma_{\mathrm{toluene}}c_{\mathrm{toluene}} + \sigma_{\mathrm{benzyl}}c_{\mathrm{benzyl}} + \sigma_{\mathrm{C_7H_6}}c_{\mathrm{C_7H_6}}))) \quad (6)$$

To model the fractional absorption in our study, we accordingly considered absorption of these species and used temperature-independent absorption cross-sections

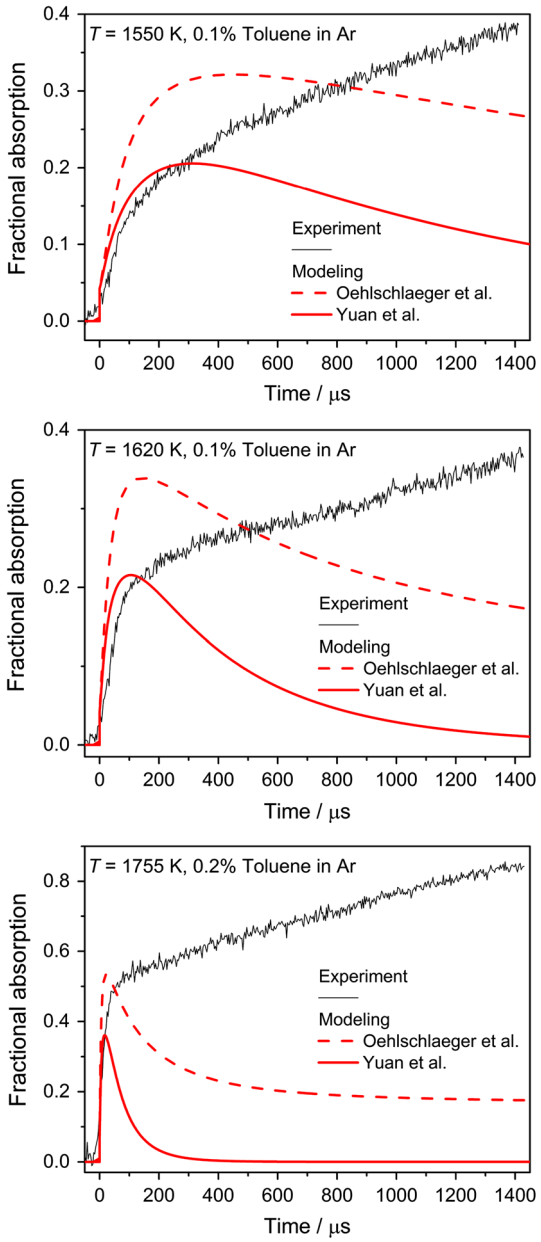

Fig. 8 Comparison of the measured fractional absorption with model predictions based on the mechanisms of Oehlschlaeger et al. [20] and Yuan et al. [25, 26] considering contributions to the absorption from toluene, benzyl, and C_7H_6 according to Eq. 6

at 266 nm from Ref. [20]: $\sigma_{\mathrm{toluene}} = 5.9 \times 10^{-19}$ cm^2, $\sigma_{\mathrm{benzyl}} = 1.9 \times 10^{-17}$ cm^2, and $\sigma_{C_7H_6} = 3.4 \times 10^{-18}$ cm^2. Note that Oehlschlaeger et al. [20] did not further specify which species C_7H_6 corresponds to. Derudi et al. [24] found that benzyl decomposes to o-benzyne (o-C_6H_4) + CH_3 and fulvenallene (C_7H_6) + H with a ~1:1 branching ratio, and both fulvenallene and o-benzyne likely contribute to the absorption from the product(s) of benzyl decomposition observed by Oehlschlaeger et al.

The results are shown in Fig. 8. Before arrival of the reflected shock wave (i.e., at $t < 0$), absorption by toluene is negligible compared to the absorption after the shock wave. After the reflected shock arrival, the absorption increases, which is caused to a large degree by formation of benzyl radicals. Benzyl has a strong broadband absorption in the 245–275 nm range [32, 33] and a factor of ~30 higher cross-section at 266 nm than toluene in our temperature range. The mechanism of Oehlschlaeger et al. qualitatively describes the experimentally observed initial rise in the fractional absorption, but it overpredicts the experimental results after the steep initial rise. This overestimation indicates a too high benzyl concentration predicted by this model. Toward later times, the model predicts a decreasing fractional absorption due to consumption of benzyl radicals, whereas the experimental absorption keeps increasing. This discrepancy is a clear indication of absorption of intermediates and/or products formed during toluene pyrolysis, which are not considered in Eq. 6.

We additionally modeled the fractional absorption experiments based on the very recently published toluene pyrolysis and oxidation mechanism of Yuan et al. [25, 26]. The latter contains a more comprehensive set of secondary reactions and has been validated toward a wide variety of experimental targets, overall showing remarkable performance. At all three temperatures considered, the magnitude of the initial rise predicted by the mechanism of Yuan et al. is consistent with the experimental results (cf. Fig. 8). Similar to the mechanism of Oehlschlaeger et al., the modeled absorption based on the mechanism of Yuan et al. underpredicts the measured profiles toward later times, which, again, is a sign of absorption of additional species not considered in Eq. 6. The faster decrease in the model of Yuan et al. compared to the model of Oehlschlaeger et al. is caused by a more rapid consumption of benzyl radials. At all three temperatures, both models show a faster rise than is observed experimentally. This effect might be caused by the limited time resolution of our detection system (~70 µs, see Sect. 2).

Figure 9 shows the predicted time profiles based on the mechanism of Yuan et al. at the three temperatures considered. For clarity, only species with a maximum concentration of 3 % relative to the initial toluene concentration are plotted. At all three temperatures, the peak concentration of phenyl radicals is more than an order of magnitude less than that of benzyl, although both radicals are formed in similar amounts (with a preference for benzyl) from the initial unimolecular decomposition of toluene via R1a and R1b, respectively [20, 34]. This result is consistent with the phenyl radical being more reactive than the resonantly stabilized benzyl radical and justifies that phenyl has not been considered in Eq. 6. Due to the small absorption cross-section of benzene (~2×10^{-20} cm^2 at 266 nm [20]), neglecting its contributions to the observed fractional absorption is justified as well.

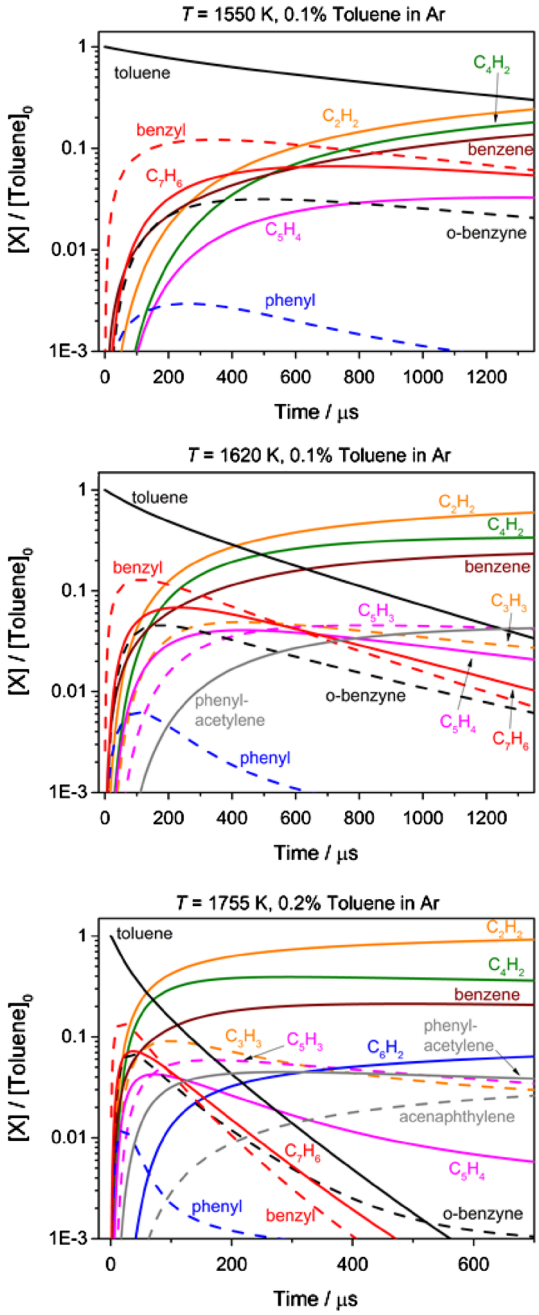

Fig. 9 Modeled concentration–time profiles for the three experiments shown in Fig. 8, based on the mechanism of Yuan et al. [25, 26]. Only species which have a maximum concentration above 3 % relative to the initial toluene concentration at $t = 0$ are shown for clarity. H_2, CH_3, and CH_4 are also not plotted for clarity, although, except for CH_3 at 1,550 K, their concentrations exceed 3 %. Here, C_7H_6 represents fulvenallene

According to Fig. 9, the model predicts substantial formation of acetylene (C_2H_2) and polyacetylenes (C_4H_2 and C_6H_2), the formation of the latter becoming more prominent

with increasing temperature. To the best of our knowledge, their UV absorption cross-sections at high temperature have not been reported in the literature. Whereas C_2H_2 does not absorb at 266 nm at room temperature, unpublished measurements from our laboratory showed fluorescence of C_2H_2 after 266-nm laser excitation at $T > 1{,}200$ K. These results suggest non-negligible absorption at 266 nm at these conditions, presumably caused by a redshift of the strong absorption band located at room temperature below 200 nm. This effect might become more pronounced with increasing temperature. C_4H_2 and C_6H_2 absorb at 266 nm already at room temperature ($\sigma_{C_4H_2}(293\ \mathrm{K}) \sim 2 \times 10^{-20}$ cm^2 [35] (using the value reported at 264 nm, the upper wavelength range of their study) and $\sigma_{C_6H_2}(293\ \mathrm{K}) = 2.1 \times 10^{-19}$ cm^2 [36]) and might show even stronger absorption at higher temperature, again assuming a redshift of the absorption band located at lower wavelength [35, 36] with increasing temperature.

Previous studies have investigated the decomposition pathways of toluene and the growth of polycyclic aromatics using mass spectroscopy and gas chromatography [29, 37, 38]. These studies revealed the formation of various aromatic species, e.g., benzene, naphthalene, indene, phenylacetylene, biphenyl, dibenzyl, acenaphthylene, and fluorene. Our modeling based on the mechanism of Yuan et al. [25, 26] predicts formation of phenylacetylene and acenaphthylene in significant amounts toward the higher temperature end. As for C_2H_2 and the polyacetylenes, their absorption cross-sections at high temperature are not known.

To summarize, the absorption of acetylene, polyacetylenes, substituted and polycyclic aromatics, and potentially of soot formed via subsequent reactions must also be considered in order to adequately describe the fractional absorption during toluene decomposition at high temperature. A realistic modeling of the fractional absorption requires the knowledge of the UV absorption cross-sections of these species at high temperatures. Spectroscopic information of these species at high temperature is scarce and mostly restricted to conditions near room temperature [39–41]. Measurements of their UV absorption cross-sections at higher temperature would clearly be desirable.

3.2 LIF measurements

LIF spectra of toluene were measured as a function of temperature between 865 and 1,750 K upon 266-nm excitation at total pressures near 1 and 3 bar with argon as the bath gas. The signal was detected spectrally resolved at distinct reaction times. Figure 10 shows LIF spectra recorded at 110 µs after passage of the reflected shock wave as a function of temperature. At 865 K, toluene LIF occurs in the 270–320-nm wavelength range with a peak at around 290 nm. With increasing temperature, the LIF spectrum of toluene shifts to the red and becomes spectrally broader.

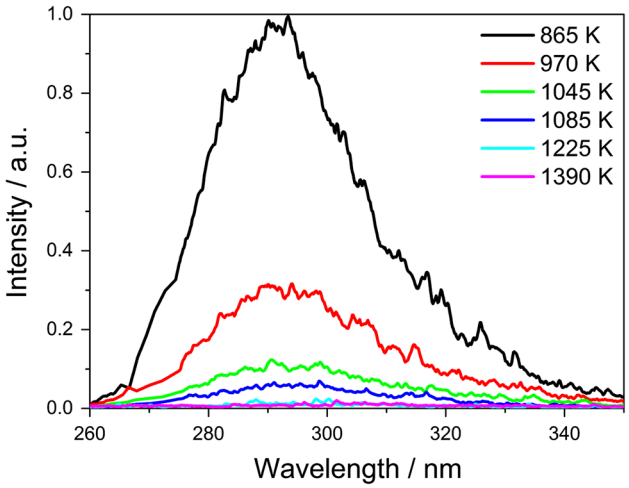

Fig. 10 Single-shot LIF emission spectra of toluene after excitation at 266 nm as a function of temperature at a pressure of 1.2 bar measured at 110 µs after the arrival of the reflected shock wave

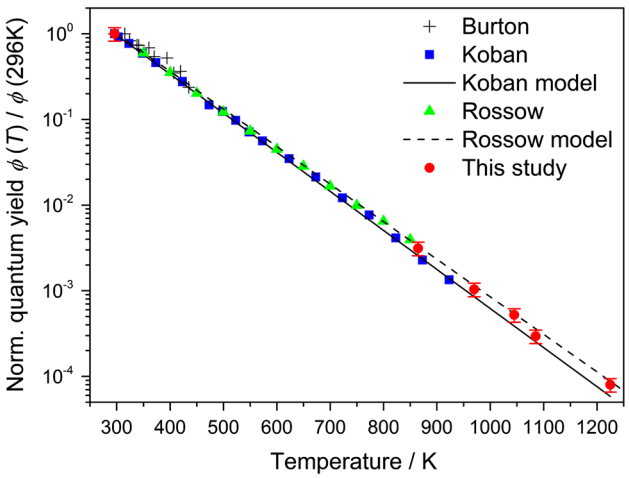

Fig. 11 Relative fluorescence quantum yield of toluene as a function of temperature. Results from the present work are compared with previous data from Burton et al. [30], Koban et al. [19], and Rossow [42]

Moreover, the fluorescence intensity decreases rapidly as a result of the decreasing fluorescence quantum yield.

Figure 11 shows the relative fluorescence quantum yield calculated (see Sect. 2) based on the fluorescence measurements and the absorption cross-sections from Fig. 5. These data extend the temperature range experimentally studied so far and can aid the development of parametric models to predict the fluorescence quantum yield. The model of Koban et al. [19] was developed from data obtained in flow cell experiments in a bath of nitrogen at total pressures of 1 bar. According to this model, the fluorescence quantum yield of toluene decreases by three orders of magnitude when increasing the temperature from room temperature

up to about 950 K. Extrapolations to higher temperatures based on this model underpredict our measured absolute values by ~20 %. In contrast, extrapolations based on the single exponential fluorescence decay approximation by Rossow [42] overestimate the measured data by ~10 %. Considering the error of ±18 % in our determinations of the fluorescence quantum yield, both models are in satisfactory agreement with our results.

To better visualize the spectral variation of the LIF of toluene and of possible decomposition products toward higher temperature, the spectra were smoothed by a FFT filter [43] with a window size of 7 nm and normalized to their respective peak intensities. The results are shown in Fig. 12. Between 865 and 1,225 K, the fluorescence maximum shows a slight redshift of about 2 nm per 100 K that follows the trend for lower temperatures reported earlier [19, 23]. Between 1,225 and 1,390 K, a significant redshift of the spectrum occurs indicating that newly formed pyrolysis products contribute to the observed LIF. This observation is qualitatively consistent with increase in the effective absorption cross-section at 266 nm (cf. Fig. 7).

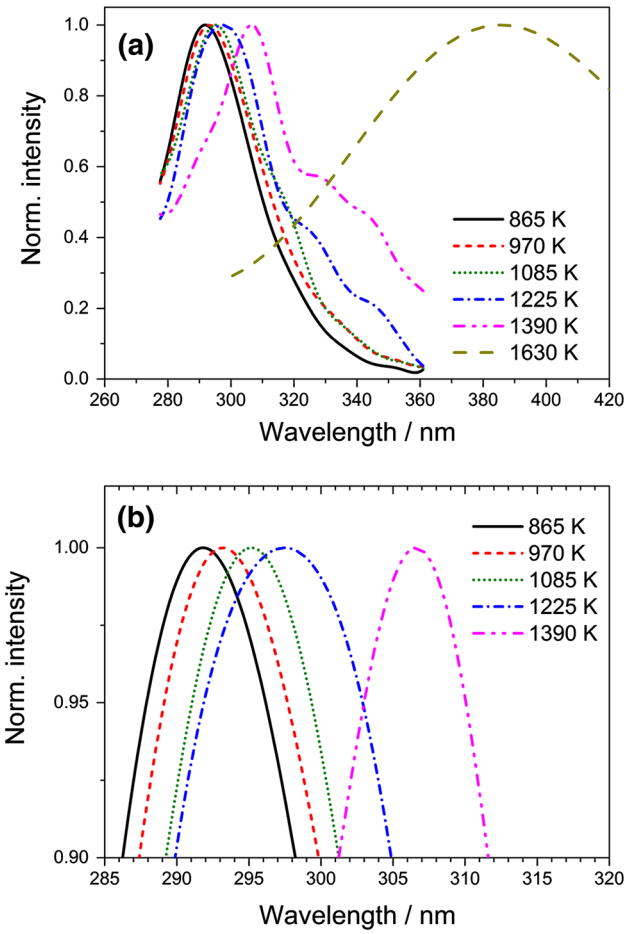

Fig. 12 Smoothed and normalized LIF emission spectra after excitation at 266 nm (see text for details on the smoothing procedure). The spectra from 865 to 1,390 K are the smoothed versions of the data from Fig. 10, taken after excitation at 110 µs after arrival of the reflected shock wave. The spectrum at 1,630 K was taken after excitation at 160 µs after the reflected shock wave (cf. Fig. 14). **a** Full spectra, **b** zoomed-in version of the 865–1,390 K spectra highlighting the *redshift* in the peak maxima

Figure 13 shows LIF spectra from experiments at 1,630 and 1,750 K. Both the shape of the spectra and the position of the emission maximum change significantly compared to lower temperatures. The toluene emission spectrum disappears completely, and new spectral features appear far redshifted compared to the original toluene spectrum as a result of the built-up of new species. The LIF emission spectrum at $T > 1{,}600$ K exhibits peak intensities comparable to the LIF intensity of toluene at lower temperature. At 1,630 K, the first strong detectable signal of pyrolysis products shows a broadband emission spectrum with a peak around 420 nm and a FWHM of 140 nm. At 1,750 K, presumably additional pyrolysis products contribute to the LIF signal, whereas at this temperature the relative signal intensity at lower wavelength decreases due to reaction progress and/or change in the fluorescence quantum yield.

Sirignano et al. [44] investigated the formation of aromatic species and soot in an atmospheric pressure counter-flow diffusion flame of ethylene using spectrally and time-resolved LIF and laser-induced incandescence (LII) measurements employing 266-nm laser light. They found different types of high molecular mass aromatic compounds.

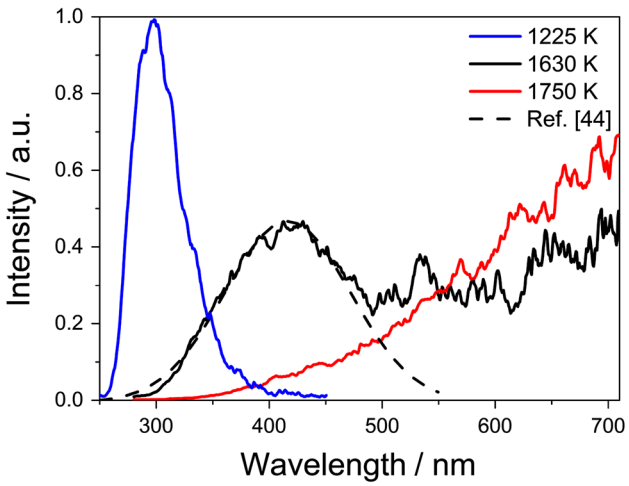

Fig. 13 LIF emission spectra of a mixture of 1 % toluene in argon at a total pressure of 2.9 bar taken after 266-nm laser excitation at 260 µs after the passage of the reflected shock wave. The spectrum at 1,225 K represents the LIF spectrum of pure toluene at this temperature. The substantial change in the spectral shape at the higher two temperatures reflects thermal decomposition of toluene and the emission of products formed from pyrolysis. The increased noise in the data after ~500 nm is caused by reduced sensitivity of the detection system. The *dashed line* shows a normalized LIF emission spectrum from Sirignano et al. [44]

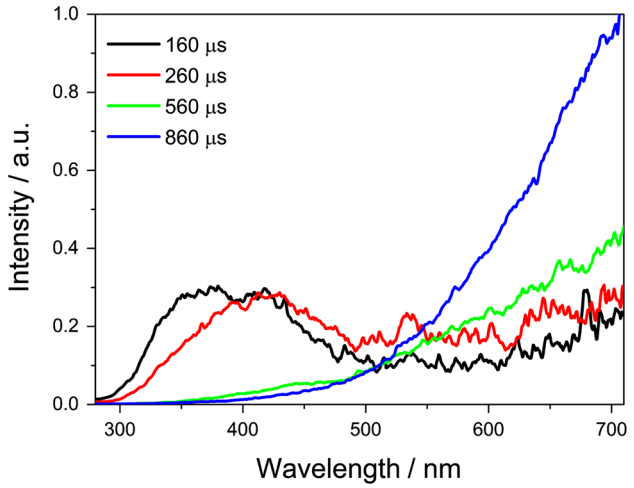

Fig. 14 LIF emission spectra of pyrolysis products after thermal decomposition of 1 % toluene in Ar at 1,630 K and a total pressure of 2.9 bar and various delay times after the passage of the reflected shock wave after 266-nm excitation

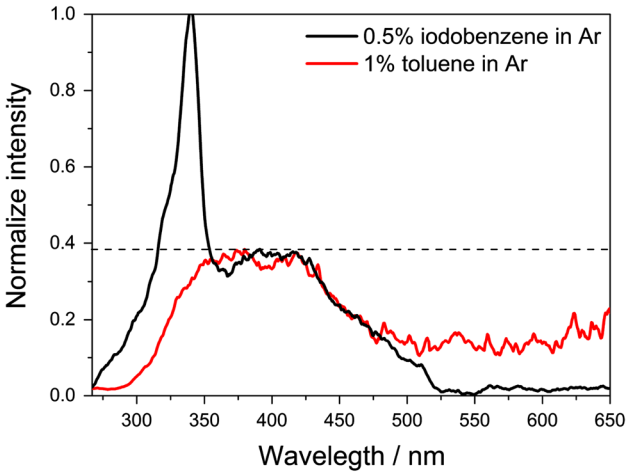

Fig. 15 Comparison of the LIF emission spectra from pyrolysis of iodobenzene and toluene at 1,630 K, 160 µs after the passage of the reflected shock wave with 266-nm laser excitation. Total pressures were 1.2 bar (iodobenzene) and 2.9 bar (toluene). Both spectra are normalized to the maximum of the broadband emission feature for better comparison

The dashed line in Fig. 13 illustrates the fitted LIF emission spectra from Ref. [44] near the stagnation plane where benzene and PAHs have their maximum concentrations. The spectrum shows a broad fluorescence emission between 290 and 550 nm, which was assigned to both small clusters of PAHs and the formation of higher molecular weight aromatic compounds. For the sake of comparison, fluorescence signals of Sirignano et al. [44] and of this study were normalized to their respective peak values. The good agreement of the spectral shapes suggests the presence of similar species in both studies at the respective conditions.

To determine the influence of toluene decomposition and formation of pyrolysis products on the LIF signal, separate experiments were performed at constant temperature (1,630 K), in which the LIF was excited at different times (160, 260, 560, and 860 µs) after the reflected shock wave. The results are shown in Fig. 14. At 160 µs, emission was observed with a peak around 375 nm and a FWHM of 135 nm. At 260 µs, the emission is shifted to the red and becomes spectrally significantly broadened toward longer times (560 and 860 µs). This behavior suggests that the emission is a superposition from several species, such as various single- or polyaromatic hydrocarbons. It may be speculated that this signal is mostly caused by larger PAH molecules. The shape of the spectrum taken at 860 µs suggests that at least a part of the emission is caused by black-body radiation originating from LII of soot particles. Sirignano et al. [44] verified that at longer wavelengths (>500 nm), their spectrum maximizes due to the incandescence emission of solid particles. It should be kept in mind that some of the aromatic molecules like indene and phenylacetylene discussed above (see Sect. 2.1) are soot precursors [29]. These species are formed behind reflected shock waves, according to the most recent mechanism published by Zhang et al. [45] and Matsugi et al. [22], and as predicted by our modeling based on the mechanism of Yuan et al. [25, 26].

To identify to which extent phenyl radicals or products from their reactions might contribute to the observed fluorescence signal during toluene pyrolysis at high temperatures, we performed additional experiments using iodobenzene (C_6H_5I), which is a clean high-temperature source of phenyl radicals [46, 47]. Figure 15 shows the LIF spectrum obtained after decomposition of iodobenzene (black line) at 1,630 K in comparison with the fluorescence signal during toluene decomposition under comparable conditions. The sharp peak in the iodobenzene spectrum around 340 nm originates from iodine atoms [48], and its width reflects the spectral instrument function. Interestingly, the spectra from both toluene and iodobenzene decomposition show a similar broadband emission feature between ~300 and 500 nm. In contrast, the emission at wavelengths above ~500 nm observed in the toluene experiment cannot be reproduced in the iodobenzene experiment. Experiments using a selective benzyl radical precursor, e.g., benzyl iodide, are necessary to further assess whether (a) phenyl or its reaction products selectively cause the feature between 300 and 500 nm and (b) benzyl or its reaction products are responsible for the emission at longer wavelength. These experiments are reserved for future work.

4 Conclusions

Time-resolved UV absorption and single-shot LIF spectra of toluene and its decomposition products were

recorded behind reflected shock waves over a wide temperature range (810–1,755 K) and near atmospheric pressures (1.2–2.9 bar). In the absorption experiments up to 1,140 K, where toluene is stable within the test time, the width of the absorption spectrum increased and showed a slight redshift as a function of temperature. Because of rapid formation of benzyl radicals from decomposition of toluene at higher temperatures combined with their large UV absorption cross-section, a pronounced early-time increase in the fractional absorption was observed. Modeling using chemical kinetics mechanisms for toluene pyrolysis from the literature [20, 25, 26] and the high-temperature absorption cross-sections of toluene, benzyl, and C_7H_6 as a product from benzyl decomposition predicted the early-time increase reasonably well but significantly underestimated the experimental absorption toward later times. This discrepancy suggests additional absorption of intermediates and products under our pyrolytic conditions.

The LIF emission spectra upon 266-nm excitation taken between 865 and 1,225 K showed a redshift of the peak signal of ~2 nm per 100 K and a decreasing intensity with temperature. This decrease is caused by a decreasing fluorescence quantum yield of toluene with temperature. Relative fluorescence quantum yields were determined between 865 and 1,225 K, increasing the upper temperature limit by ~300 K compared to literature measurements. Our measurements show that the dependence of the fluorescence quantum yield on temperature remains single exponential up to at least 1,225 K. This result is consistent with literature measurements taken at lower temperature and confirms predictions of parametric models. Above 1,300 K, the LIF spectra showed a significant redshift. Above 1,600 K, we observed a strong signal increase, with the signal being orders of magnitude stronger than the nascent toluene fluorescence expected in the same temperature range by extrapolation of the temperature-dependent fluorescence cross-section. Both effects are presumably from contribution of species of the pyrolysis process.

The dependence of photo-physical properties of toluene on temperature and pressure in a reaction environment investigated here is of great interest for practical tracer-LIF applications. Our work provides validation data for a model-based understanding of toluene as a tracer in O_2-free environments and reveals an important role of pyrolysis products on the absorption and fluorescence properties. Future investigations need to elucidate the potential of the nascent pyrolysis species for diagnostics applications.

Acknowledgments The authors gratefully acknowledge the financial support by the Deutsche Forschungsgemeinschaft (DFG) within the project SCHU1369/9.

References

1. H. Neij, B. Johansson, M. Aldén, Combust. Flame **99**, 449 (1994)
2. C. Schulz, V. Sick, Prog. Energy Combust. Sci. **31**, 75 (2005)
3. M. Luong, R. Zhang, C. Schulz, V. Sick, Appl. Phys. B **91**, 669 (2008)
4. D.A. Rothamer, J.A. Snyder, R.K. Hanson, R.R. Steeper, R.P. Fitzgerald, Proc. Combust. Inst. **32**, 2869 (2009)
5. S.A. Kaiser, M. Schild, C. Schulz, Proc. Combust. Inst. **34**, 2911 (2013)
6. F. Großmann, P.B. Monkhouse, M. Ridder, V. Sick, J. Wolfrum, Appl. Phys. B **62**, 249 (1996)
7. W. Koban, J.D. Koch, R.K. Hanson, C. Schulz, Appl. Phys. B **80**, 147 (2005)
8. N. Graf, J. Gronki, C. Schulz, T. Baritaud, J. Cherel, P. Duret, J. Lavy, SAE technical paper series 2001-01-1924 (2001)
9. V. Sick, C.K. Westbrook, Proc. Combust. Inst. **32**, 913 (2009)
10. P. Tröndle, R. Schießl, U. Maas, in *Studies on the interference of nascent acetone to tracer LIF in IC-engines*, Proceedings of the Fifth European Combustion Meeting (Cardiff, 2011)
11. M. Hartmann, I. Gushterova, M. Fikri, C. Schulz, R. Schießl, U. Maas, Combust. Flame **158**, 172 (2011)
12. M. Fikri, L.R. Cancino, M. Hartmann, C. Schulz, Proc. Combust. Inst. **34**, 393 (2013)
13. C. Schulz, J. Gronki, S. Andersson, SAE technical paper series 2004-01-1917 (2004)
14. M. Richter, J. Engström, A. Franke, M. Aldén, A. Hultqvist, B. Johansson, SAE technical paper series 2000-01-2868 (2000)
15. S. Faust, T. Dreier, T. Dreier, C. Schulz, Chem. Phys. **383**, 6 (2011)
16. J.D. Koch, R.K. Hanson, Appl. Phys. B **76**, 319 (2003)
17. M. Orain, P. Baranger, B. Rossow, F. Grisch, Appl. Phys. B **102**, 163 (2012)
18. J. Trost, L. Zigan, S.C. Eichmann, T. Seeger, A. Leipertz, Appl. Opt. **52**, 6300 (2013)
19. W. Koban, J.D. Koch, R.K. Hanson, C. Schulz, Phys. Chem. Chem. Phys. **6**, 2940 (2004)
20. M.A. Oehlschlaeger, D.F. Davidson, R.K. Hanson, Proc. Combust. Inst. **31**, 211 (2007)
21. W. Koban, J.D. Koch, R.K. Hanson, C. Schulz, Appl. Phys. B **80**, 777 (2005)
22. A. Matsugi, A. Miyoshi, Proc. Combust. Inst. **34**, 269 (2013)
23. S. Faust, G. Tea, T. Dreier, C. Schulz, Appl. Phys. B **110**, 81 (2013)
24. M. Derudi, D. Polino, C. Cavallotti, Phys. Chem. Chem. Phys. **13**, 21308 (2011)
25. W. Yuan, Y. Li, P. Dagaut, J. Yang, F. Qi, Combust. Flame **162**, 3 (2015)
26. W. Yuan, Y. Li, P. Dagaut, J. Yang, F. Qi, Combust. Flame **162**, 22 (2015)
27. R.J. Kee, F.M. Rupley, J.A. Miller, M.E. Coltrin, J.F. Grcar, E. Meeks, H.K. Moffat, A.E. Lutz, G. Dixon-Lewis, M.D. Smooke, J. Warnatz, G.H. Evans, R.S. Larson, R.E. Mitchell, L.R. Petzold, W.C. Reynolds, M. Carcotsios, W.E. Stewart, P. Glarborg, C. Wang, O. Adigun, *CHEMKIN Collection* (Reaction Design Inc., San Diego, CA, 2009)
28. J.E.A. John, T.G. Keith, *Gas Dynamics* (Prentice Hall, Englewood Cliffs, NJ, 2006)
29. R. Sivaramakrishnan, R.S. Tranter, K. Brezinsky, J. Phys. Chem. A **110**, 9388 (2006)
30. C.S. Burton, W.A. Noyes, J. Chem. Phys. **49**, 1705 (1968)
31. M. Fikri, M. Hartmann, C. Schulz, *Temporally- and spectrally-resolved UV absorption measurements of toluene during pyrolysis in shock-heated gases* (European Combustion Meeting, Cardiff, Great Britain, 2011)
32. N. Ikeda, N. Nakashima, K. Yoshihara, J. Phys. Chem. **88**, 5803 (1984)

33. W. Müller-Markgraf, J. Troe, J. Phys. Chem. **92**, 4899 (1988)
34. S.J. Klippenstein, L.B. Harding, Y. Georgievskii, Proc. Combust. Inst. **31**, 221 (2007)
35. N.S. Smith, Y. Bénilan, P. Bruston, Planet Space Sci. **46**, 1215 (1998)
36. Y. Bénilan, P. Bruston, F. Raulin, R. Courtin, J.C. Guillemin, Planet Space Sci. **43**, 83 (1995)
37. B. Shukla, A. Susa, A. Miyoshi, M. Koshi, J. Phys. Chem. A **111**, 8308 (2007)
38. T.C. Zhang, L.D. Zhang, X. Hong, K.W. Zhang, F. Qi, C.K. Law, T.H. Ye, P.H. Zhao, Y.L. Chen, Combust. Flame **156**, 2071 (2009)
39. T.J. Wallington, H. Egsgaard, O.J. Nielsen, J. Platz, J. Sehested, T. Stein, Chem. Phys. Lett. **290**, 363 (1998)
40. A. Le Person, G. Eyglunent, V. Daële, A. Mellouki, Y. Mu, J. Photochem Photobiol. A: Chem. **195**, 54 (2008)
41. R.K. Abhinavam Kailasanathan, J. Thapa, F. Goulay, J. Phys. Chem. A **118**, 7732–7741 (2014)
42. B. Rossow, *Photophysical Processes of Organic Fluorescent Molecules and Kerosene—Applications to Combustion Engines* (Université Paris-Sud, Paris, 2011)
43. E.O. Brigham, *The Fast Fourier Transform and Its Applications* (Prentice-Hall Inc, Englewood Cliffs, NJ, 1988)
44. M. Sirignano, A. Collina, M. Commodo, P. Minutolo, A. D'Anna, Combust. Flame **159**, 1663 (2012)
45. L. Zhang, J. Cai, T. Zhang, F. Qi, Combust. Flame **157**, 1686 (2010)
46. D. Robaugh, W. Tsang, J. Phys. Chem. **90**, 5363 (1986)
47. S.S. Kumaran, M.-C. Su, J.V. Michael, Chem. Phys. Lett. **269**, 99 (1997)
48. J.C.G. Martín, J. Blahins, U. Gross, T. Ingham, A. Goddard, A.S. Mahajan, A. Ubelis, A. Saiz-Lopez, Atmos. Meas. Tech. **4**, 29 (2011)